IEEE Access
Multidisciplinary ⋮ Rapid Review ⋮ Open Access Journal

Received January 6, 2022, accepted February 1, 2022, date of publication February 10, 2022, date of current version March 1, 2022.

Digital Object Identifier 10.1109/ACCESS.2022.3150830

Motion State Recognition and Trajectory Prediction of Hypersonic Glide Vehicle Based on Deep Learning

JUNBIAO ZHANG[1], JIAJUN XIONG[1], LINGZHI LI[1], QIUSHI XI[1], XIN CHEN[1], AND FAN LI[2]
[1]Early Warning Information Department, Early Warning Academy, Wuhan 430000, China
[2]Unit 95980 of PLA, Xiangyang 441100, China

Corresponding author: Junbiao Zhang (zhangjb95@126.com)

This work was supported in part by the National High-Tech Research and Development Program of China under Grant 2015AA7056045 and Grant 2015AA8017032P, and in part by the Postgraduate Funding Project of China under Grant JY2019B138.

ABSTRACT Hypersonic glide vehicle (HGV) has brought severe challenges to the existing defense system due to its characteristics of high maneuverability, high speed and high precision. Simultaneously, these characteristics also bring great difficulties to trajectory prediction. In this paper, a method for HGV motion state recognition and trajectory prediction based on deep learning is proposed. The proposed method consists of two modules, namely the motion state recognition module and the trajectory prediction module. The motion state recognition module can identify the HGV's motion state according to state information, and divide it into eight categories. The softmax function is added to the state recognition module to calculate the probability of each motion state. The trajectory prediction module comprises a nonlinear prediction part and a linear prediction part. According to the result of motion state recognition, the appropriate prediction scheme is adopted to better extract the linear and nonlinear characteristics of HGV trajectory, which improves the robustness and prediction accuracy of the proposed method. The experimental results of HGV trajectory prediction show that the proposed method can maintain good stability when the HGV maneuver state changes, and has higher accuracy than the four benchmark methods.

INDEX TERMS Hypersonic glide vehicle, trajectory prediction, sequence to sequence, deep learning, state recognition.

I. INTRODUCTION

HGV is an aircraft with a speed above Mach 5 and flying in near space [1]. Compared with a conventional ballistic missile, HGV has stronger maneuverability and can strike any target in the world within two hours [2]. It has changed the traditional combat style and has significant military application value, which has attracted the great attention of various countries [3], [4]. At this time, the high speed and high maneuverability of HGV also bring difficulties to its trajectory prediction.

Trajectory prediction refers to the prediction of a target's motion trajectory or trend within a period of time in the future [5]. The trajectory of HGV is different from that of the aircraft and the ballistic missile, which has the characteristic of ''jumping'' in the longitudinal direction and can maneuver in a wide range in the lateral direction. Thus the trajectory prediction of HGV is more complicated.

Presently, related studies on HGV trajectory prediction have rarely been reported, and the existing researches mainly adopt parameter extrapolation or data-driven methods. The method based on parameter extrapolation mainly achieves trajectory prediction by establishing a dynamic or kinematic model to estimate and extrapolate the parameters. Wang *et al.* [6] proposes a trajectory prediction method that combines the flight state and flight intention of HGV, and verifies the effectiveness of the method in simulation experiments. However, it is sometimes difficult to judge flight intention in practice. Han *et al.* [7] achieves the prediction of HGV in the height direction through the autoregressive moving average model, but it could be unable to obtain the three-dimensional state of HGV. Zhai *et al.* [8] defines a set of new aerodynamic parameters, and extrapolates them based on the least square method to realize the trajectory

The associate editor coordinating the review of this manuscript and approving it for publication was Ehab Elsayed Elattar.

prediction of HGV. Li *et al.* [9] proposes a trajectory prediction method based on empirical mode decomposition of aerodynamic acceleration, and extrapolates the aerodynamic acceleration by the least square method to realize trajectory prediction. In addition, the data-driven method mainly realizes trajectory prediction through machine learning or deep learning [10], [11]. Yang and He [12] applies the generalized regression neural network to the HGV trajectory prediction by taking advantage of its nonlinear advantages, thus reducing the prediction error. Cheng *et al.* [13] proposes a HGV trajectory prediction algorithm combining support vector machine and extended Kalman filter, and conducts trajectory prediction experiments under balanced gliding and jumping gliding of HGV, respectively. The above studies have made much progress in the trajectory prediction of HGV, but there are still some limitations. On the one hand, the above methods are based on the historical motion state of HGV, which will seriously affect the prediction effect when the HGV maneuver state changes. On the other hand, the above methods can only achieve trajectory prediction in a short period of time, and the prediction accuracy is not satisfactory.

In recent years, deep learning networks such as recurrent neural networks [14], convolutional neural networks [15], [16] and long short-term memory networks [17], [18] have attracted wide attention, and have shown good performance in feature extraction, pattern recognition and time series prediction [19]–[23]. In this paper, a motion state recognition and trajectory prediction method of HGV is proposed based on deep learning theory. In order to verify the proposed method, we conduct simulation experiments on radar tracking data and compare the performance with the current mainstream methods. The main contributions of this paper are as follows.

a) Five identification parameters are selected from the HGV state information by analyzing its maneuvering characteristics and control parameter model, and the HGV motion state can be effectively judged based on them.

b) A motion state recognition model based on the ConvLSTM network is designed, which can automatically extract the characteristics of HGV motion trajectory and classify the maneuvering state through the softmax classifier.

c) A trajectory prediction method based on motion state recognition is proposed, including a nonlinear feature extraction module and a linear feature extraction module. The nonlinear feature extraction module is composed of a seq2seq network structure, and the linear feature extraction module is composed of a perceptron. Thus, the proposed method can flexibly select the prediction scheme according to the motion state of HGV, and has better accuracy.

The rest of this paper is organized as follows. Section 2 creates the motion equation and control parameter model of HGV, and introduces the details of the establishment of the trajectory library. Section 3 introduces the specific details of the motion state recognition and trajectory prediction method of HGV. Section 4 verifies the performance of the proposed method through simulation experiments. Section 5 concludes the paper.

II. PRELIMINARIES

In this section, we introduce some background technologies of HGV, including the equation of motion, the longitudinal and lateral control parameters model, and the establishment of the trajectory library. These background technologies are the theoretical basis for HGV trajectory prediction.

A. THE EQUATION OF MOTION

In the Velocity-Turn-Climb (VTC) coordinate system, assuming that the earth model is a uniform sphere, the formula of six-freedom motion of HGV is established without considering the effect of earth's oblateness [24], [25].

$$\begin{cases} \dot{r} = v\sin\theta \\ \dot{\lambda} = \dfrac{v\cos\theta\sin\sigma}{r\cos\phi} \\ \dot{\phi} = \dfrac{v\cos\theta\cos\sigma}{r} \\ \dot{v} = -a_D - g\sin\theta \\ \dot{\theta} = \dfrac{a_L\cos v}{v} + \dfrac{v\cos\theta}{r} - \dfrac{g\cos\theta}{v} \\ \dot{\sigma} = \dfrac{a_L\sin v}{v\cos\theta} + \dfrac{v\cos\theta\sin\sigma\tan\phi}{r} \end{cases} \tag{1}$$

where r, λ, φ, v, θ and σ are state variables of HGV, which denote the geocentric distance, longitude, latitude, velocity, velocity inclination and velocity course angle, respectively. ω_e is the earth rotation rate. a_L is the aerodynamic lift acceleration. a_D is the aerodynamic drag acceleration. The expressions of aerodynamic lift acceleration and aerodynamic drag acceleration are expressed as follows:

$$\begin{cases} a_L = \dfrac{L}{m} = \dfrac{1}{2}\rho v^2 \cdot \dfrac{C_L(\alpha)S}{m} \\ a_D = \dfrac{D}{m} = \dfrac{1}{2}\rho v^2 \cdot \dfrac{C_D(\alpha)S}{m} \end{cases} \tag{2}$$

where L is the aerodynamic lift, D is the aerodynamic drag, $C_L(\alpha)$ is the aerodynamic lift coefficient, $C_D(\alpha)$ is the aerodynamic drag coefficient. α and v are the control parameters, representing the attack angle and the bank angle, respectively. S is the HGV reference area. ρ is the atmospheric density. m is the HGV mass.

B. CONTROL PARAMETER MODELING

The HGV trajectory can be divided into a longitudinal trajectory and a lateral trajectory. By stacking the maneuvers in two directions, more complex maneuvers can be realized to increase the flexibility of the HGV trajectory, thereby avoiding the detection and no-fly zones. Next, we will introduce the longitudinal and lateral control parameters model.

1) LONGITUDINAL CONTROL PARAMETER MODEL

There are two main maneuvering states of HGV in the longitudinal direction, namely balanced gliding state and

jumping gliding state. In the balanced gliding state, the force on HGV in the longitudinal direction is balanced, and the changing rate of velocity inclination is zero. According to the motion equation of HGV, the control parameter model under the condition of balanced gliding state should satisfy the following equation [26]:

$$\frac{L\cos\upsilon}{mv}+\frac{1}{v}\left(\frac{v^2}{r}-g\right)\cos\theta=0 \tag{3}$$

In addition, the longitudinal aerodynamic force of HGV is also impacted by the attack angle. HGV can achieve balanced gliding in the longitudinal direction only when the change rate of velocity inclination angle is equal to zero and the attack angle remains constant at the same time.

If the conditions of balanced gliding are not satisfied, HGV will be in the state of jumping gliding. HGV can change the jump amplitude and jump frequency through the change of the attack angle. Since the speed of HGV during the initial gliding phase is relatively high, the aerodynamic heat is the main constraint that affects the flight. A larger attack angle should be used to increase the altitude of the lowest point when the HGV descends. As the speed of HGV decreases, aerodynamic heat is no longer the main constraint. In order to increase the range of HGV, the attack angle should be adjusted to increase the lift-drag ratio as much as possible. Therefore, the attack angle is modelled as a function of speed.

$$\alpha_c=\begin{cases}\alpha_{\max}\\ \alpha_{\text{mid}}+\alpha_{\text{bal}}\sin\left[\dfrac{\pi}{v_1-v_2}(v-v_{\text{mid}})\right]\\ \alpha_{\max(L/D)}\end{cases} \tag{4}$$

$$\alpha_{\text{mid}}=\left(\alpha_{\max}+\alpha_{\max(L/D)}\right)/2 \tag{5}$$

$$\alpha_{\text{bal}}=\left(\alpha_{\max}-\alpha_{\max(L/D)}\right)/2 \tag{6}$$

$$v_{\text{mid}}=(v_1+v_2)/2 \tag{7}$$

where $\alpha_{\max}$ and $\alpha_{\max(L/D)}$ are the maximum attack angle and the maximum lift-drag ratio attack angle, respectively. L/D is the lift-drag ratio.

2) LATERAL CONTROL PARAMETER MODEL

The lateral maneuver of HGV is mainly affected by the bank angle. In order to improve the offensive and defensive ability, HGV can perform a variety of lateral maneuvers, such as no maneuver, C-shaped maneuver, and S-shaped maneuver.

No lateral maneuver can reduce the kinetic energy consumption of HGV and increase the range, but it will also increase the probability of being intercepted. The bank angle is usually set to zero when HGV is no maneuver in the lateral direction. The C-shaped maneuver generally refers to left-turn or right-turn, and the trajectory is relatively stable. The bank angle is usually set to a constant when HGV is a C-shaped maneuver in the lateral direction. The S-shaped maneuver refers to HGV makes multiple turns in the lateral direction, which can increase its maneuverability. The bank angle should be reversed several times when HGV performs a S-shaped maneuver. The model of bank angle is defined as:

$$v_c=\begin{cases}v_c, & \Delta\sigma_{threshold}<\Delta\sigma\\ v_c^-, & -\Delta\sigma_{threshold}\le\Delta\sigma\le\Delta\sigma_{threshold}\\ -v_c, & \Delta\sigma<-\Delta\sigma_{threshold}\end{cases} \tag{8}$$

where $\Delta\sigma_{threshold}$ is the error threshold of the velocity course angle. v_c^- is the bank angle of HGV at the previous moment.

TABLE 1. Initial parameter range of the trajectory.

Initial Parameter	Symbol	Value
Height	h_0	40-70 km
Velocity	v_0	3000-6000 m/s
Longitude	λ_0	0°
Latitude	ϕ_0	0°
Velocity inclination	θ_0	-0.1-0°
Velocity course angle	σ_0	-15-15°
Surface area	S	0.4839 m^2
Mass	m	907 kg

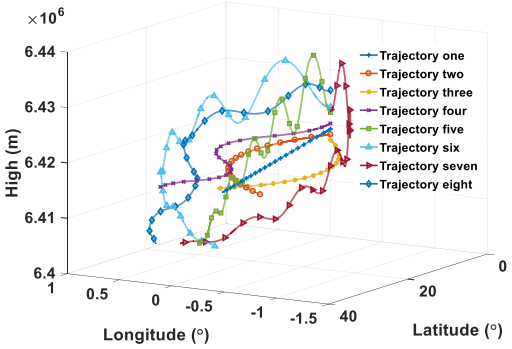

FIGURE 1. Typical maneuver trajectories of HGV.

3) ESTABLISHMENT OF TRAJECTORY LIBRARY

Various maneuver trajectories of HGV can be generated by designing different initial variables and different control parameter models. The HGV trajectory library generated in this paper contains 2,430 trajectories with a total of 4.734 million trajectory points, covering all kinds of maneuvering modes of HGV. The value range of the initial parameters of HGV is shown in Table 1. Several typical maneuvering trajectories are shown in Figure 1.

III. METHODOLOGY

In this section, we introduce the overall idea of HGV trajectory prediction. The trajectory prediction method based on motion state recognition is proposed, and the technical details of the motion state recognition module and the trajectory prediction module are reported, respectively.

A. FRAMEWORK

HGV has strong maneuverability and diverse motion states. Its three-dimensional trajectory can be decomposed in the longitudinal direction and lateral direction, as shown in

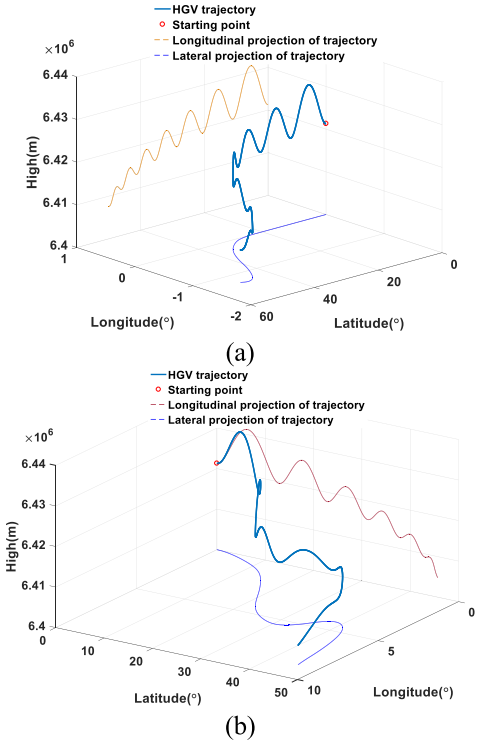

FIGURE 2. HGV 3D maneuver trajectory decomposition. (a) Turning maneuver trajectory decomposition. (b) Weaving maneuver trajectory decomposition.

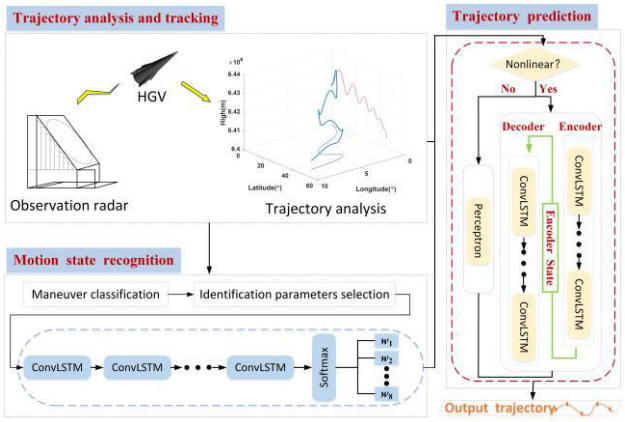

FIGURE 3. Framework of the trajectory prediction method.

Figure 2. It can be seen that the HGV maneuver trajectory has both nonlinear and linear characteristics. Therefore, the trajectory features of HGV cannot be well extracted by simply using a nonlinear model or linear model. It is necessary to design a trajectory prediction network that can extract both nonlinear and linear features, and select the appropriate prediction scheme according to the motion state of HGV. So a trajectory prediction method based on motion state recognition is proposed. The proposed method includes two parts, namely the motion state recognition module and the trajectory prediction module, and its structure is shown in Figure 3.

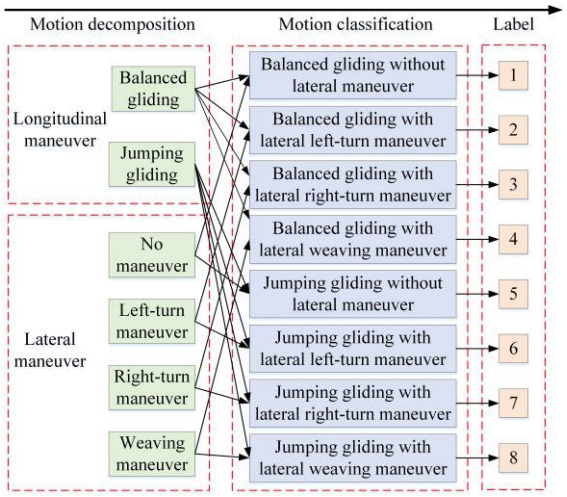

FIGURE 4. HGV maneuver classification.

The motion state recognition module takes identification parameters as input, extracts the data change characteristics through a deep neural network, and uses the softmax function to output the probability corresponding to each motion state of HGV.

The trajectory prediction module comprises a nonlinear prediction part and a linear prediction part, which improves the accuracy and robustness of the proposed method. In this way, the proposed method can extract the nonlinear and linear features and better deal with trajectory prediction in the simple maneuver state and complex maneuver state of HGV.

B. MOTION STATE RECOGNITION MODULE

1) MOTION STATE CLASSIFICATION

The maneuver of HGV in the longitudinal direction can be divided into balanced gliding and jumping gliding, and the maneuver in the lateral direction can be divided into no maneuver, left-turn maneuver, right-turn maneuver and weaving maneuver. Therefore, eight maneuver categories can be obtained by combining the longitudinal and lateral maneuvers of HGV, as shown in Figure 4.

2) INDENTIFICATION PARAMETERS SELECTION

According to the relevant knowledge of flight dynamics [27], the HGV maneuvering process is accompanied with the change of various parameters, including height, height change rate, velocity inclination, velocity course angle and the change rate of velocity course angle. The height, height change rate and velocity inclination are mainly sensitive to the maneuver of HGV in the longitudinal direction. The velocity course angle and the change rate of velocity course angle are mainly sensitive to the maneuver of HGV in the lateral direction.

Height is the vertical distance between the center of mass and ground. Height change rate can be obtained by the

difference method, and the equation is

$$\Delta h = \frac{\mathrm{d}h}{\mathrm{d}t} = \frac{h(t_{k+1}) - h(t_k)}{t_{k+1} - t_k} \tag{9}$$

where t_k is the current time.

The velocity inclination refers to the angle between the velocity axis and horizontal direction, which is positive upward and negative downward. The velocity course angle refers to the angle between the projection of velocity on the horizontal plane and the due north direction, which is positive to the right and negative to the left. The change rate of velocity course angle can also be obtained by the difference method.

Next, the variation law of each identification parameter will be introduced when HGV performs different maneuvers in the longitudinal and lateral directions. When HGV is in a balanced gliding state in the longitudinal direction, the height and the height change rate change smoothly, and the velocity inclination is close to zero. When HGV is in a jumping gliding state in the longitudinal direction, the height, height change rate and velocity inclination all oscillate regularly. When HGV has no lateral maneuver, the velocity course angle remains unchanged, and the change rate of velocity course angle is basically zero. When HGV turns left, the velocity course angle decreases continuously, and the change rate of velocity course angle is negative. When HGV turns right, the velocity course angle increases continuously, and the change rate of velocity course angle is positive. When HGV performs weaving maneuver, the velocity course angle and the change rate of velocity course angle change in oscillating. Accordingly, the mapping relationship between HGV maneuver state and identification parameters can be analyzed. The change of identification parameters can be captured by the state recognition method, and the maneuver state of HGV can be judged.

3) MOTION STATE RECOGNITION MODEL

The identification parameters constructed in this paper are multidimensional time series data, which can fully reflect the motion characteristics of HGV, and has both temporal and spatial characteristics. Combining the advantages of convolutional neural network (CNN) in local feature extraction [28] and long short-term memory network (LSTM) in time series processing [18], [29], a state recognition model based on convolutional long short-term memory network (ConvLSTM) is designed.

ConvLSTM combines the advantages of LSTM and CNN, and its main improvement is that the convolution operation is used to replace the matrix multiplication operation in LSTM [30]. The network structure of LSTM and ConvLSTM is shown in Figure 5. Therefore, it can better extract the characteristics and laws of time series information, and has been widely concerned in time series classification and prediction. The specific calculation process of ConvLSTM is described as follows:

$$\boldsymbol{i}_t = \sigma\left(\boldsymbol{W}_{xi} * \boldsymbol{X}_t + \boldsymbol{W}_{hi} * \boldsymbol{H}_{t-1} + \boldsymbol{b}_i\right) \tag{10}$$

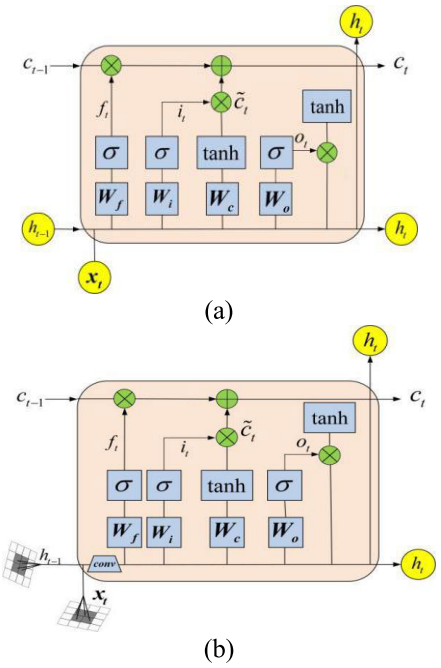

FIGURE 5. The network structure of LSTM and ConvLSTM. (a) LSTM network structure. (b) ConvLSTM network structure.

$$\boldsymbol{f}_t = \sigma\left(\boldsymbol{W}_{xf} * \boldsymbol{X}_t + \boldsymbol{W}_{hf} * \boldsymbol{H}_{t-1} + \boldsymbol{b}_f\right) \tag{11}$$

$$\boldsymbol{o}_t = \sigma\left(\boldsymbol{W}_{x0} * \boldsymbol{X}_t + \boldsymbol{W}_{h0} * \boldsymbol{H}_{t-1} + \boldsymbol{b}_0\right) \tag{12}$$

$$\hat{\boldsymbol{C}}_t = \tanh\left(\boldsymbol{W}_{xc} * \boldsymbol{X}_t + \boldsymbol{W}_{hc} * \boldsymbol{H}_{t-1} + \boldsymbol{b}_c\right) \tag{13}$$

$$\boldsymbol{C}_t = \boldsymbol{f}_t \circ \boldsymbol{C}_{t-1} + \boldsymbol{i}_t \circ \hat{\boldsymbol{C}}_t \tag{14}$$

$$\boldsymbol{H}_t = \boldsymbol{o}_t \circ \tanh \boldsymbol{C}_t \tag{15}$$

where $\boldsymbol{X}_t$ is the current input, $\boldsymbol{H}_{t-1}$ and $\boldsymbol{H}_t$ represent the output of the previous moment and the current moment, respectively. $\boldsymbol{C}_{t-1}$ and $\boldsymbol{C}_t$ represent the cell state at the previous time and the cell state at the current time, respectively. $\boldsymbol{C}_t$ represents newly generated information. $\boldsymbol{W}_{xi}, \boldsymbol{W}_{hi}, \boldsymbol{W}_{xf}, \boldsymbol{W}_{lf}, \boldsymbol{W}_{x0}, \boldsymbol{W}_{h0}, \boldsymbol{W}_{xc}, \boldsymbol{W}_{hc}, \boldsymbol{b}_i, \boldsymbol{b}_f, \boldsymbol{b}_0$ and $\boldsymbol{b}_c$ are corresponding weight matrices and offset vectors, respectively. σ represents sigmoid function. tanh and * represent tanh function and convolution operation, respectively. o represents the element-by-element multiplication.

Then, the ConvLSTM network output is connected to the full connection layer, and the HGV motion is classified by the softmax activation function to obtain the corresponding probability of each motion state. The calculation formula is defined as follows:

$$\boldsymbol{P}_i = \mathrm{softmax}\left(\boldsymbol{W}_x * \boldsymbol{H}_t + \boldsymbol{b}_x\right) \tag{16}$$

where $\boldsymbol{W}_x$ and $\boldsymbol{b}_x$ are the weight matrix and offset vector of the softmax layer, respectively.

The input of the motion state recognition model is a multidimensional data group composed of identification parameters, and the output is the probability vector corresponding to the motion state category. In order to improve the efficiency of the model, the output probability vector

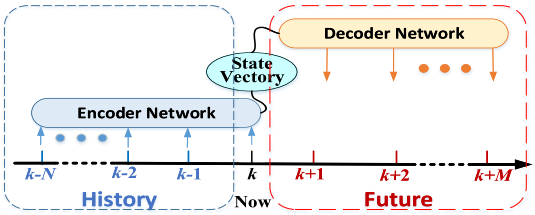

FIGURE 6. The seq2seq model structure.

is further processed. When the maximum value of the probability vector is greater than or equal to 80%, it is adjusted to 100%, and the probability value corresponding to the rest states is zero. At this time, the output is a one-hot vector. When the maximum value of the probability vector is less than 80%, the elements are arranged and accumulated from large to small, and stop when the cumulative value is greater than or equal to 80%. The elements participating in the accumulation are normalized, and the remaining elements are set to zero. At this time, the output is a new probability vector.

C. TRAJECTORY PREDICTION MODULE

The input of the trajectory prediction module includes the output of the motion state recognition module and the historical trajectory information of HGV, and the output is the predicted trajectory of HGV. The trajectory of HGV can be decomposed into the lateral trajectory and longitudinal trajectory. We first predict the trajectory of HGV in the lateral plane and longitudinal plane, respectively, and then combine them into three-dimensional coordinates of HGV. Since the HGV trajectory has both linear and nonlinear characteristics, the trajectory prediction module consists of a linear prediction part and a nonlinear prediction part.

1) NONLINEAR PREDICTION PART

The nonlinear prediction part is designed as a sequence to sequence (seq2seq) architecture [31]. The seq2seq model can extract the hidden data rules, especially when the length of the input sequence and the output sequence are different. So it is suitable for capturing the hidden laws in the HGV trajectory [32], [33]. It usually consists of two parts: an encoder and a decoder. The structure is shown in Figure 6.

During encoding, a fixed-dimensional vector $\boldsymbol{C}_{\text{enc},k}$, which is called a semantic vector, can be generated by the encoder from the input information of HGV trajectory $x_{k-N}, x_{k-N+1}, \cdots, x_k$. It contains the hidden features of HGV trajectory changing with time. During decoding, the decoder takes the semantic vector as the initial hidden state. The features of the input information can be extracted to realize trajectory prediction by decoding the semantic vector. The whole working process can be simplified as follows:

$$\begin{cases} \boldsymbol{C}_{\text{enc},k} = \text{Encoder}\left(x_{k-N}, x_{k-N+1}, \cdots, x_k\right) \\ P\left(x_k, x_{k+1}, \cdots, x_{k+M} \mid x_{k-N}, x_{k-N+1}, \cdots, x_k\right) \\ \qquad = \text{Decoder}\left(\boldsymbol{C}_{\text{enc},k}\right) \end{cases} \tag{17}$$

where Encoder$(\cdot)$ represents an encoding network, Decoder$(\cdot)$ represents a decoding network, $\boldsymbol{C}_{\text{enc},k}$ is the context vector passed between the encoder and the decoder. $(x_{k-N}, x_{k-N+1}, \cdots, x_k)$ represents the input sequence. $(x_k, x_{k+1}, \cdots, x_{k+M})$ represents the output sequence. k is the current moment. N and M represent the sequence length of the input and output, respectively.

The encoder and decoder networks can be designed as RNN or LSTM, or other types of networks. In this paper, the encoding and decoding networks are designed as ConvLSTM networks because the motion trajectory of HGV has temporal and spatial characteristics. The calculation process of the ConvLSTM network has been introduced in Section 3.2.3.

To increase the judgement ability of the decoder output, the self-attention mechanism is added to calculate the weight of each state of the encoder. The weight value corresponding to each state vector is calculated by the softmax function [34].

$$a_k = \frac{\exp(e_k)}{\sum_k e_k} \tag{18}$$

where a_k represents the weight value of the k-th state vector. e_k is the score function, which is expressed as

$$e_k = \boldsymbol{V}^T \tanh(\boldsymbol{W}^T \boldsymbol{h}_i + \boldsymbol{b}) \tag{19}$$

where $\boldsymbol{V}$, $\boldsymbol{W}$ and $\boldsymbol{b}$ are parameters that can be learned during model training. T represents matrix transpose.

2) LINEAR PREDICTION PART

A complex model maybe not the best model, and only a suitable model can produce the best results. The linear prediction part is added to the trajectory prediction model mainly to compensate for the strong nonlinear characteristics of the complex neural network model. We design the linear prediction part as a perceptron, and set the number of network layers to one. The calculation process can be expressed as follows:

$$\boldsymbol{Y}_t = \boldsymbol{W}_t \boldsymbol{X}_t + \boldsymbol{b}_t \tag{20}$$

where $\boldsymbol{W}_t$ and $\boldsymbol{b}_t$ are the weight matrix and offset vector, respectively.

IV. EXPERIMENTS

In this section, we design an experiment to verify the prediction performance of the proposed method. The experiment is carried out in three typical HGV flight scenarios.

A. EXPERIMENTAL DETAILS

1) EXPERIMENTAL DATA

This experiment is carried out in two steps. The first step is to verify the motion state recognition ability of the model. The second step is to verify the trajectory prediction ability of the model.

The data used in the motion state recognition module is the trajectory library data established in section 2.2.3. The data set contains the state information and identification parameters information of HGV. The samples of 80% are

TABLE 2. Parameter settings of HGV trajectory.

Initial parameter	Parameter settings of trajectory one	Parameter settings of trajectory two	Parameter settings of trajectory three
Height	50 km	55 km	45 km
Velocity	5000 m/s	6000 m/s	4500 m/s
Longitude	0°	0°	0°
Latitude	0°	0°	0°

TABLE 3. Parameter settings of radar and environment.

Parameter type	Parameter	Value
Radar Parameters	Sampling interval	0.5 s
	Geographic coordinates	[12°, 1.5°, 1 km]
	Distance error	200 m
	Azimuth error	0.15°
	Pitch angle error	0.15°
Environmental parameters	Atmospheric density constant	1.22 kg/m^3
	Earth gravitational constant	3.99×10^{14} N·m^2/kg
	Earth rotation rate	7.29×10^{-5} rad/s
	Earth radius	6378 m

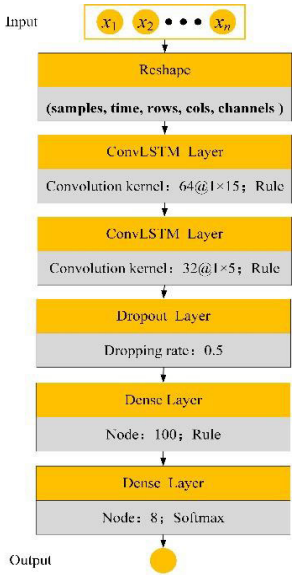

FIGURE 7. Hierarchical structure of motion state recognition model.

selected as the training data and the remaining 20% are selected as the verification data.

The data used in the trajectory prediction module is the radar tracking data. We verify the performance of the trajectory prediction method in three typical HGV flight scenarios, respectively. The parameter settings of the three HGV trajectories are shown in Table 2. Trajectory one is the trajectory of HGV in a simple maneuver state, trajectory two is the trajectory of HGV in a complex maneuver state. The parameter settings of the observation radar and the external environment are shown in Table 3. The method in the Ref. [22] is used to filter the radar observations to obtain the tracking trajectory.

2) EVALUATION CRITERION

In order to objectively evaluate the prediction performance of the model, two indicators are used to measure the error of trajectory prediction, namely root mean square error (RMSE) and mean square error (MAE). The formula is defined as follows:

$$\mathrm{RMSE} = \sqrt{\frac{1}{N}\sum_{i=1}^{N}(X_P - X_t)^2} \tag{21}$$

$$\mathrm{MAE} = \frac{1}{N}\sum_{i=1}^{N}|X_P - X_t| \tag{22}$$

where X_P is the predicted position of HGV, X_t is the real position of HGV. N is the prediction duration.

3) MODEL CONFIGURATION AND TRAINING

The model code is written in Python 3.7.6 and implemented by the TensorFlow framework. The simulation is conducted on a mobile workstation with an Intel Core i7-10510U processor and 16G memory.

The network of the motion state identification module has five layers, including two ConvLSTM network layers, one dropout layer, and two full connection layers. The structure, parameters, and other configurations are shown in Figure 7.

The prediction module includes a nonlinear prediction part and a linear prediction part. The nonlinear prediction part adopts the encoder-decoder structure. The encoding network is designed as two ConvLSTM network layers. The decoding network is designed as two ConvLSTM network layers and one Dense layer. The linear prediction part consists of a perceptron. The batch size of the above network is set to 128 and the training epoch is set to 100. The time window size is 120, and the learning rate is 0.001.

In the above models, an adaptive moment estimation (Adam) optimizer is selected as the optimization method to update the parameters in the model according to the error gradient. Adam is an extension of the traditional stochastic gradient descent algorithm, which can calculate the adaptive learning rate of each parameter and make the model converge more efficiently. The cross entropy is selected as the loss function to adjust the weight update speed according to the size of the error.

B. PERFORMANCE ANALYSIS OF MOTION STATE RECOGNITION

The accuracy of motion state recognition will directly affect the performance of trajectory prediction. The high recognition accuracy can provide reliable support for trajectory prediction. The RNN model, CNN model and LSTM model are selected as comparison models, and the time step and learning rate settings are the same as those of the ConvLSTM network. These deep learning models are trained by using the data in the trajectory library. The loss curve and accuracy curve of training are shown in Figure 8. The recognition

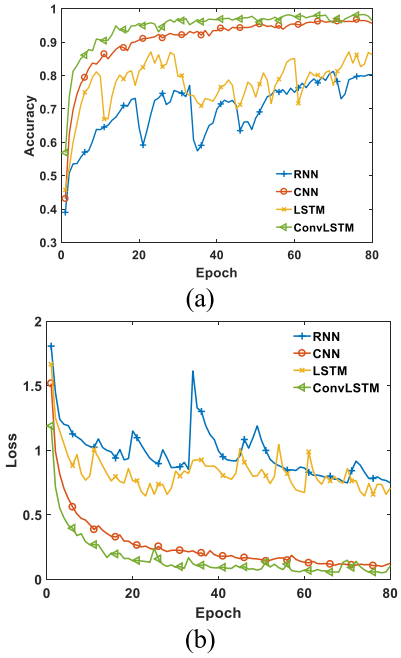

FIGURE 8. Training results of different models.

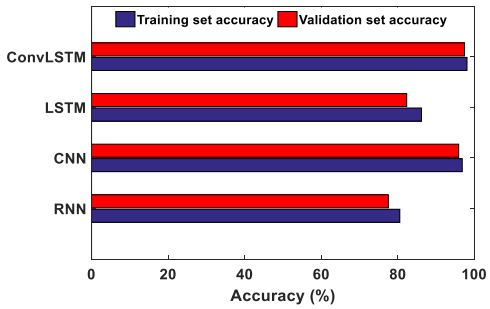

FIGURE 9. Model recognition accuracy histogram.

TABLE 4. Accuracy comparison of models.

Model	Accuracy	
	Accuracy on the training set	Accuracy on the validation set
RNN	80.51%	77.51%
CNN	96.83%	95.89%
LSTM	86.18%	82.31%
ConvLSTM	98.06%	97.41%

accuracy of the ConvLSTM model on the training set and the validation set is shown in Table 4, which can be visually displayed in the form of a histogram, as shown in Figure 9.

It can be seen that the accuracy of the RNN model and LSTM model is significantly lower than that of the other two models, which indicates that although the RNN model and LSTM model have advantages in dealing with long-term dependence problems, they cannot extract data features well. CNN model can better extract local features through convolution operation, and has achieved high accuracy in the training and verification set. However, the recognition

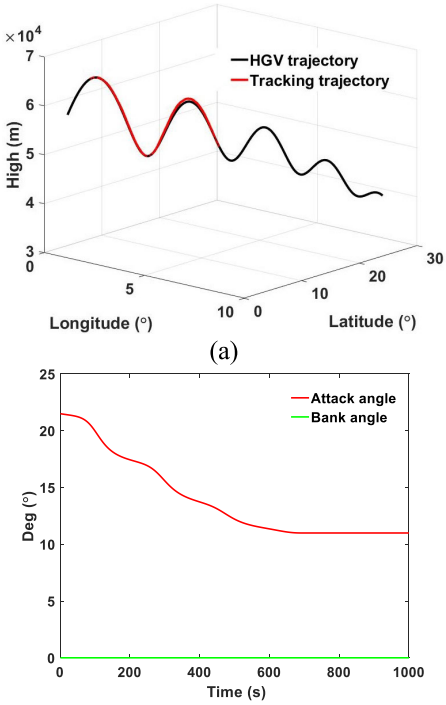

FIGURE 10. Trajectory one. (a) The real trajectory and tracking trajectory. (b) Changes of control parameters.

accuracy rate of the ConvLSTM model is the highest. It achieves 97.41% accuracy on the verification set, and has the best recognition effect on the motion state of HGV.

C. PERFORMANCE ANALYSIS OF TRAJECTORY RREDICTION

1) BENCHMARK MODELS

In order to verify the prediction effect of the proposed model, the following benchmark models are selected for comparison: ConvLSTM model Chen *et al.* [35], SA-ConvLSTM model Li *et al.* [36], SS-DLSTM model Zeng *et al.* [37] and EMD_AA model Li *et al.* [9]. ConvLSTM model is a widely used comparison method. SA-ConvLSTM model and SS-DLSTM model represent the most advanced methods in recent years. EMD_AA model is the current mainstream non-neural network method for trajectory prediction. The hyper parameters of ConvLSTM model, SA-ConvLSTM model and SS-DLSTM model are derived by the trial-and-error method. The function design in EMD_AA model is the same as that in literature [9]. Each model is run ten times and the average value is taken for comparison.

The simulation is carried out on three types of HGV trajectories, respectively. The performances of different models are compared.

2) TRAJECTORY RREDICTION OF JUMPING GLIDING WITHOUT LATERAL MANEUVER

The real trajectory and tracking trajectory of HGV in the jumping gliding without lateral maneuver state are shown

TABLE 5. Comparison of model prediction accuracy of trajectory one.

Method	Evaluation index	Longitudinal direction			Lateral direction			Total		
		30 s	60 s	90 s	30 s	60 s	90 s	30 s	60 s	90 s
ConvLSTM	RMSE / m	206	498	697	2575	3419	3661	2583	3454	3726
	MAE / m	192	426	640	2535	3350	3555	2542	3377	3612
SS_DLSTM	RMSE / m	205	504	560	2570	3099	3275	2578	3139	3322
	MAE / m	189	461	521	2544	3053	3237	2551	3087	3279
SA_ConvLSTM	RMSE / m	137	314	416	2491	3093	3253	2495	3108	3279
	MAE / m	122	289	364	2461	3039	3188	2464	3053	3208
EMD_AA	RMSE / m	862	807	778	2236	2537	3145	2396	2662	3240
	MAE / m	845	789	760	2232	2508	3006	2387	2629	3101
Proposed model	RMSE / m	107	255	339	1570	1797	2271	1574	1815	2296
	MAE / m	102	217	296	1542	1716	2049	1545	1729	2070

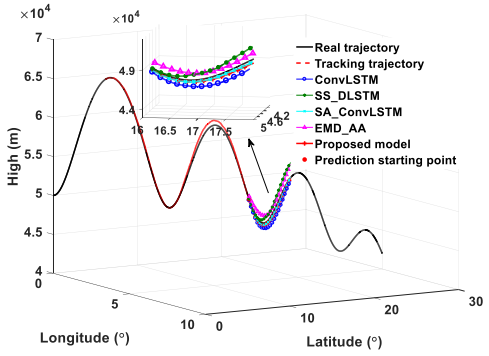

FIGURE 11. The prediction of trajectory one.

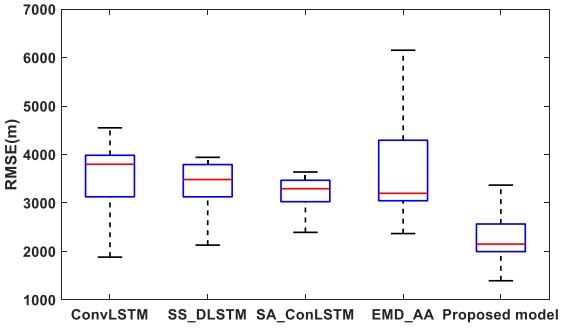

FIGURE 12. The prediction error boxplot of trajectory one.

in Figure 10(a), and the corresponding control variables are shown in Figure 10(b).

The proposed method and the benchmark models are used to predict trajectory one, and the result is shown in Figure 11.

The RMSE and MAE values of each model in the longitudinal and lateral directions are calculated, as shown in Table 5, where the prediction duration is set to 90 s. It can be seen that the prediction performance of the deep learning model is better than those of the EMD_AA model in the longitudinal direction. This is because the longitudinal trajectory of HGV is nonlinear, and the deep learning model has a stronger fitting ability and feature extraction ability for nonlinear data. However, the prediction results of the deep learning model are generally worse in the lateral direction. The reason may be that the lateral trajectory of HGV is linear, and the linear prediction part is needed to compensate for the nonlinear characteristics of the complex neural networks.

In addition, it can be noted that the lateral prediction error of HGV is much larger than the longitudinal prediction error. The reason is that the longitudinal maneuver range of the HGV is basically within 60km. In contrast, the lateral maneuver range reaches thousands of kilometers, which is much larger than the longitudinal maneuver range. Therefore, a small prediction error in the lateral will cause a significant decrease in accuracy. Meanwhile, the proposed model adds a linear module, so the lateral prediction error is smaller.

The prediction error boxplot is shown in Figure 12. It can be concluded that the proposed model maintains a better prediction accuracy and is better than other models. The EMD_AA method also maintains good stability when predicting the trajectory, which indicates that the EMD_AA method can deal with the trajectory prediction of HGV in the simple maneuver state.

The error boundary is analyzed according to the 3δ principle. The standard deviation between the predicted trajectory of the proposed method and the real trajectory is calculated. The longitudinal prediction error region and the lateral prediction error region are drawn, as shown in Figure 13(a) and Figure 13(b). To analysis the three-dimensional prediction error, we select seven prediction points from the prediction trajectory to compare with the real trajectory points, and the error ellipsoid is used to represent the error boundary in three directions according to the 3δ principle, as shown in Figure 13(c). It can be seen that the longitudinal prediction error region is divergent with the increase of prediction time, and the lateral prediction error region changes relatively stable because the lateral trajectory changes linearly.

3) TRAJECTORY RREDICTION OF JUMPING GLIDING WITH LATERAL WEAVING MANEUVER

The real trajectory and tracking trajectory of HGV in the jumping gliding with lateral weaving maneuver state

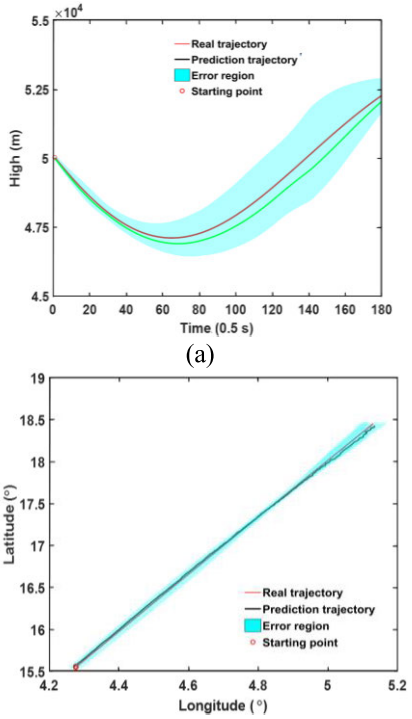

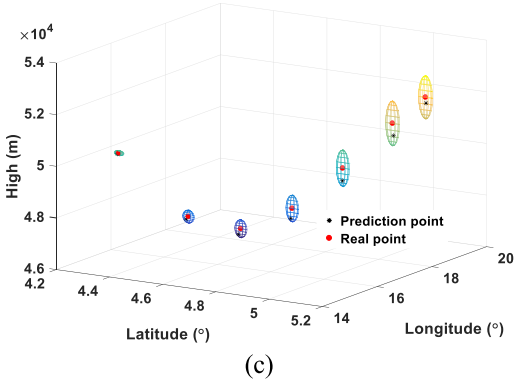

FIGURE 13. The variation of prediction error region of trajectory one. (a) The variation of longitudinal prediction error region. (b) The variation of lateral prediction error region. (c) The variation of three-dimensional prediction error ellipsoid.

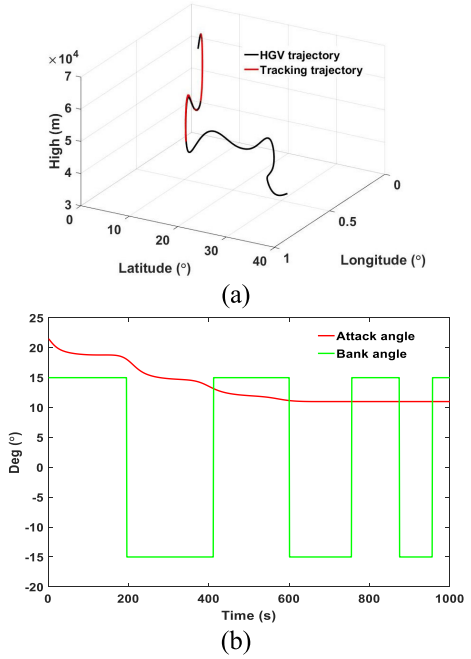

FIGURE 14. Trajectory two. (a) The real trajectory and tracking trajectory. (b) Changes of control parameters.

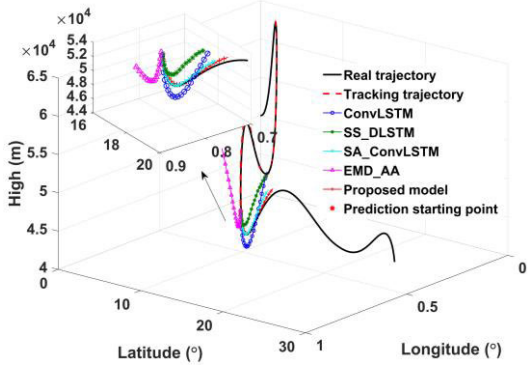

FIGURE 15. The prediction of trajectory two.

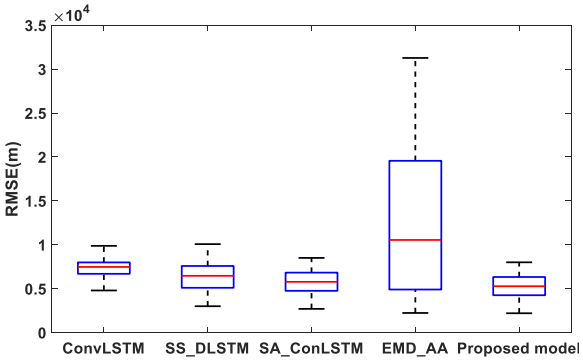

FIGURE 16. The prediction error boxplot of trajectory two.

are shown in Figure 14(a), and the corresponding control variables are shown in Figure 14(b).

The predicted trajectory is shown in Figure 15. Under the complex maneuvering mode of HGV, the proposed model adopts the nonlinear prediction part in both longitudinal and lateral directions.

The RMSE and MAE values of each model in the longitudinal and lateral directions are calculated, and the results are shown in Table 6. It can be seen that the prediction error of each model has been increased due to the complex trajectory of HGV. The prediction error of the EMD_AA model increases rapidly because the EMD_AA model assumes that the maneuver mode of HGV remains unchanged. Figure 16 shows the prediction RMSE error boxplot of HGV. The proposed model maintains the optimal accuracy in the complex maneuvering trajectory of HGV. The result shows that the proposed model can adapt to different HGV maneuvering trajectories. Compared

TABLE 6. Comparison of model prediction accuracy of trajectory two.

Method	Evaluation index	Longitudinal direction			Lateral direction			Total		
		30 s	60 s	90 s	30 s	60 s	90 s	30 s	60 s	90 s
ConvLSTM	RMSE / m	926	1273	1157	4618	5747	7149	4710	5886	7242
	MAE / m	850	1194	1041	4401	5536	636	4482	5663	6451
SS_DLSTM	RMSE / m	235	726	1057	4434	5490	6364	4441	5537	6451
	MAE / m	196	578	890	4385	5369	6117	4389	5400	6181
SA_ConvLSTM	RMSE / m	163	287	466	4364	5288	5659	4367	5296	5678
	MAE / m	149	241	384	4324	5197	5541	4326	5202	5554
EMD_AA	RMSE / m	1199	1840	3219	4713	6908	11409	4863	8149	13855
	MAE / m	1158	1715	2745	4525	6691	9062	4671	7807	11469
Proposed model	RMSE / m	132	244	393	4246	5007	5292	4248	5012	5307
	MAE / m	125	203	320	4211	4954	5253	4213	4958	5263

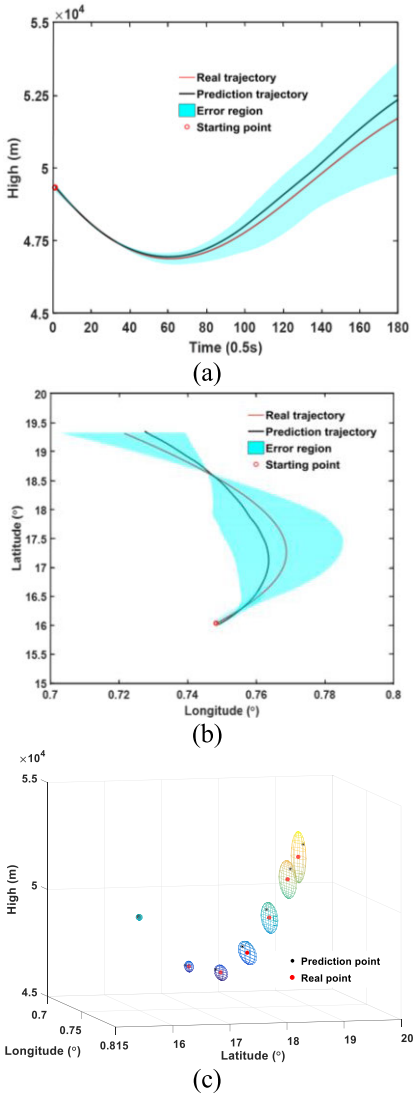

FIGURE 17. Model recognition accuracy histogram. (a) The variation of longitudinal prediction error region. (b) The variation of lateral prediction error region. (c) The variation of three-dimensional prediction error ellipsoid.

with other models, it has achieved the best prediction performance.

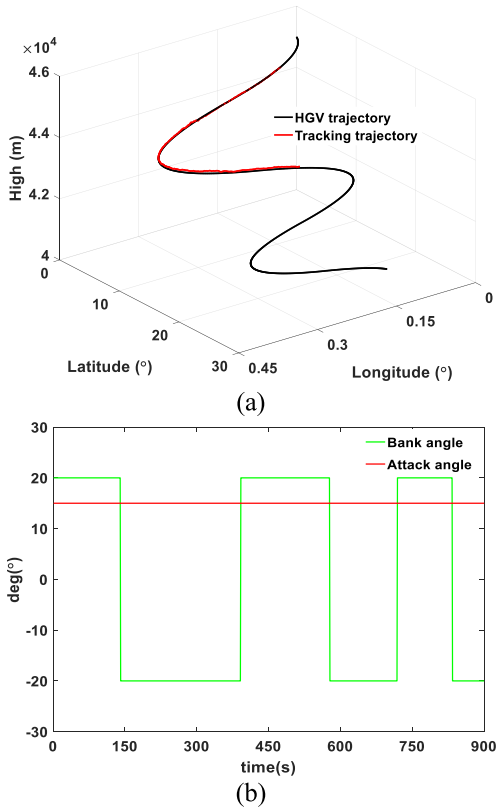

FIGURE 18. Trajectory three. (a) The real trajectory and tracking trajectory. (b) Changes of control parameters.

The error boundary between the predicted trajectory of the proposed method and the real trajectory is calculated by using the same method as in the 4.3.2 section. The longitudinal prediction error region, the lateral prediction error region and the three-dimensional prediction error ellipsoid are drawn according to the 3δ principle, as shown in Figure 17. It is clear that the longitudinal prediction error region is divergent with the increase of prediction time. Since there is an intersection between the predicted and real trajectories, the lateral prediction error region increases first, then decreases and then increases again.

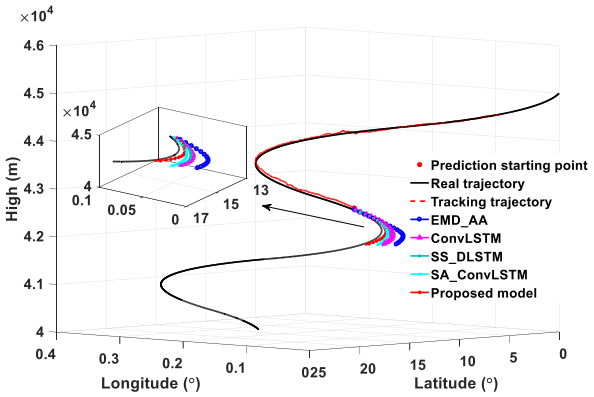

FIGURE 19. The prediction of trajectory three.

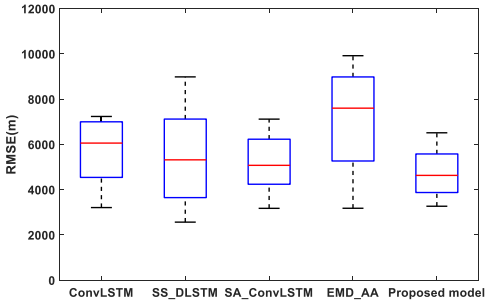

FIGURE 20. The prediction error boxplot of trajectory three.

4) TRAJECTORY RREDICTION OF BALANCED GLIDING WITH LATERAL WEAVING MANEUVER

Balanced gliding is also an important maneuvering mode for HGV. We select the balanced gliding with lateral weaving maneuver trajectory for prediction. The real trajectory and tracking trajectory are shown in Figure 18(a), and the corresponding control variables are shown in Figure 18(b).

The trajectory for the next 90 seconds is predicted and the corresponding prediction results are shown in Figure 19. The RMSE and MAE values corresponding to each model in the lateral and longitudinal directions are calculated, as shown in Table 7. Figure 20 shows the prediction RMSE error boxplot of HGV.

It can be seen that the RMSE value and MAE value of the proposed model are the smallest in both the lateral and longitudinal direction. The longitudinal prediction error region, the lateral prediction error region and the threedimensional prediction error ellipsoid are drawn according to the 3δ principle, as shown in Figure 21. The longitudinal prediction error of HGV in the balanced gliding mode is significantly lower than that in the jumping gliding mode, but the total prediction error is still large due to the weaving maneuver of HGV in the lateral direction.

The single-step time-consuming of each model is shown in Figure 22. It can be seen that the SS_DLSTM model consumes the most time due to the large number of parameters that need to be optimized. The ConvLSTM model adopts a convolution structure, which reduces the number

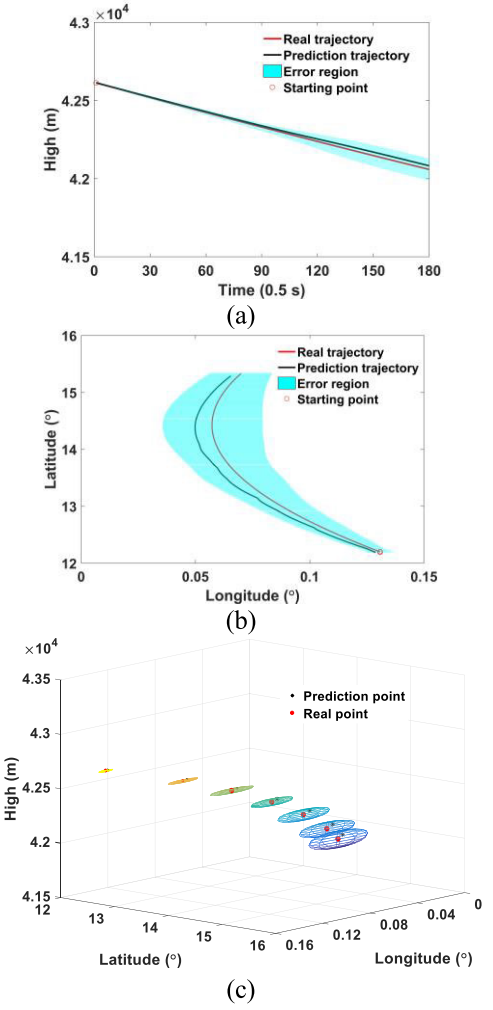

FIGURE 21. The variation of prediction error region of trajectory three. (a) The variation of longitudinal prediction error region. (b) The variation of lateral prediction error region. (c) The variation of three-dimensional prediction error ellipsoid.

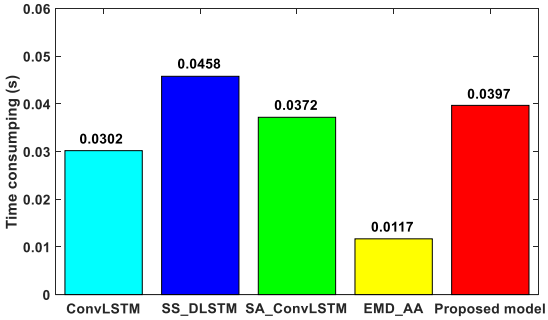

FIGURE 22. Computational complexity analysis.

of parameters, and its timeliness is better than that of SS_DLSTM. The EMD_AA model requires the least time, but it cannot cope with the trajectory prediction of HGV in the complex maneuver state. Considering the prediction effect and time consumption, the proposed model has the most application value.

TABLE 7. Comparison of model prediction accuracy of trajectory three.

Method	Evaluation index	Longitudinal direction			Lateral direction			Total		
		30 s	60 s	90 s	30 s	60 s	90 s	30 s	60 s	90 s
ConvLSTM	RMSE / m	166	201	259	3741	5096	6145	3744	5100	6150
	MAE / m	141	186	233	2329	4782	5402	2333	4785	5407
SS_DLSTM	RMSE / m	144	189	235	3063	4332	5444	3066	4334	5447
	MAE / m	132	162	211	3009	4165	5126	3012	4168	5131
SA_ConvLSTM	RMSE / m	116	137	201	2915	3997	5157	2920	4002	5163
	MAE / m	96	128	175	2755	3707	4810	2756	3709	4813
EMD_AA	RMSE / m	107	143	198	4190	6103	7676	4192	6104	8079
	MAE / m	103	125	186	3978	5754	7194	3979	5756	7597
Proposed model	RMSE / m	48	82	111	2251	3435	4756	2251	3435	4757
	MAE / m	43	76	95	2044	3008	4373	2044	3008	4374

V. CONCLUSION

In this paper, a sequence-to-sequence deep learning network model based on motion state recognition is proposed for HGV trajectory prediction. The main conclusions are as follows:

1) The current maneuver state of HGV can be effectively judged according to the identification parameters of HGV, including height, height change rate, velocity inclination, velocity course angle and the change rate of velocity course angle;

2) The trajectory prediction method based on motion state recognition can effectively reduce the prediction error caused by the HGV maneuver and has good robustness.

Meanwhile, the model also has the following limitations:

1) The model consumes a long time, and it is necessary to optimize the model further or explore a better cycle prediction scheme;

2) The prediction performance of the model is greatly affected by the training set, so it is necessary to study further how to construct and optimize the training set;

3) Trajectory prediction is realized based on the tracking data, so improving the tracking accuracy is also helpful to improve the trajectory prediction accuracy.

REFERENCES

[1] S. Li, H. Lei, L. Shao, and C. Xiao, "Multiple model tracking for hypersonic gliding vehicles with aerodynamic modeling and analysis," *IEEE Access*, vol. 7, pp. 28011–28018, 2019.

[2] F. Meng and K. Tian, "Phased-array radar task scheduling method for hypersonic-glide vehicles," *IEEE Access*, vol. 8, pp. 221288–221298, 2020.

[3] L. Song, X. Li, and Y. Liu, "Effect of time-varying plasma sheath on hypersonic vehicle-borne radar target detection," *IEEE Sensors J.*, vol. 21, no. 15, pp. 16880–16893, Aug. 2021.

[4] B. Zhang and D. Zhou, "Optimal predictive sliding-mode guidance law for intercepting near-space hypersonic maneuvering target," *Chin. J. Aeronaut.*, vol. 35, no. 4, pp. 321–331, 2022.

[5] J. Zhang, J. Liu, R. Hu, and H. Zhu, "Online four dimensional trajectory prediction method based on aircraft intent updating," *Aerosp. Sci. Technol.*, vol. 77, pp. 774–787, Jun. 2018.

[6] K. Wang, Z. Xu, S. Tang, and J. Wan, "A trajectory prediction method for near space short-range glide vehicle based on flight mission," *J. Astronaut.*, vol. 42, no. 1, pp. 50–60, 2021.

[7] C. Han, J. Xiong, K. Zhang, and X. Lan, "Decomposition ensemble trajectory prediction algorithm for hypersonic vehicle," *Syst. Eng. Electron.*, vol. 40, no. 1, pp. 151–158, 2018.

[8] D. Zhai, H. M. Lei, J. Li, and T. Liu, "Trajectory prediction of hypersonic vehicle based on adaptive IMM," *Acta Aeronaut. Astronaut. Sinica*, vol. 37, no. 11, pp. 3466–3475, 2016.

[9] L. Fan, X. Jiajun, L. Xuhui, B. Hongkui, and C. Xin, "NSHV trajectory prediction algorithm based on aerodynamic acceleration EMD decomposition," *J. Syst. Eng. Electron.*, vol. 32, no. 1, pp. 103–117, Feb. 2021.

[10] S. Mozaffari, O. Y. Al-Jarrah, M. Dianati, P. Jennings, and A. Mouzakitis, "Deep learning-based vehicle behavior prediction for autonomous driving applications: A review," *IEEE Trans. Intell. Transp. Syst.*, vol. 23, no. 1, pp. 33–47, Jan. 2022.

[11] R. Liu, M. Liang, J. Nie, W. Lim, Y. Zhang, and M. Guizani, "Deep learning-powered vessel trajectory prediction for improving smart traffic services in maritime Internet of Things," *IEEE Trans. Netw. Sci. Eng.*, early access, Jan. 7, 2022, doi: 10.1109/TNSE.2022.3140529.

[12] B. Yang and Z. He, "Hypersonic vehicle track prediction based on GRNN," *Comput. Appl. Softw.*, vol. 32, no. 7, pp. 239–243, 2015.

[13] Y. Cheng, C. Sun, and X. Yan, "Trajectory prediction of hypersonic glide vehicle based on SVM and EKF," *J. Beijing Univ. Aeronaut. Astronaut.*, vol. 46, no. 11, pp. 2094–2105, 2020.

[14] H.-F. Dai, H.-W. Bian, R.-Y. Wang, and H. Ma, "An INS/GNSS integrated navigation in GNSS denied environment using recurrent neural network," *Defence Technol.*, vol. 16, no. 2, pp. 334–340, Apr. 2020.

[15] Y. Wang, T. Liu, D. Zhang, and Y. Xie, "Dual-convolutional neural network based aerodynamic prediction and multi-objective optimization of a compact turbine rotor," *Aerosp. Sci. Technol.*, vol. 116, pp. 1–13, Sep. 2021.

[16] D. Zhou, X. Zhuang, and H. Zuo, "A hybrid deep neural network based on multi-time window convolutional bidirectional LSTM for civil aircraft APU hazard identification," *Chin. J. Aeronaut.*, vol. 35, no. 4, pp. 344–361, Apr. 2022.

[17] C. Che, H. Wang, Q. Fu, and X. Ni, "Combining multiple deep learning algorithms for prognostic and health management of aircraft," *Aerosp. Sci. Technol.*, vol. 94, pp. 1–9, Nov. 2019.

[18] S. Hochreiter and J. Schmidhuber, "Long short-term memory," *Neural Comput.*, vol. 9, no. 8, pp. 1735–1780, 1997.

[19] Y. Zhang, Y. Li, and G. Zhang, "Short-term wind power forecasting approach based on Seq2Seq model using NWP data," *Energy*, vol. 213, pp. 1–14, Dec. 2020.

[20] J.-Q. Luo, H.-S. Fang, F.-M. Shao, Y. Zhong, and X. Hua, "Multi-scale traffic vehicle detection based on faster R–CNN with NAS optimization and feature enrichment," *Defence Technol.*, vol. 17, no. 4, pp. 1542–1554, Aug. 2021.

[21] Z. Huang, A. Hasan, K. Shin, R. Li, and K. Driggs-Campbell, "Long-term pedestrian trajectory prediction using mutable intention filter and warp LSTM," *IEEE Robot. Autom. Lett.*, vol. 6, no. 2, pp. 542–549, Apr. 2021.

[22] S. Ghimire, Z. M. Yaseen, A. A. Farooque, R. C. Deo, J. Zhang, and X. Tao, "Streamflow prediction using an integrated methodology based on convolutional neural network and long short-term memory networks," *Sci. Rep.*, vol. 11, no. 1, pp. 1–26, Dec. 2021.

[23] R. Ma, X. Zheng, P. Wang, H. Liu, and C. Zhang, "The prediction and analysis of COVID-19 epidemic trend by combining LSTM and Markov method," *Sci. Rep.*, vol. 11, no. 1, pp. 1–14, Dec. 2021.

[24] J. Zhang, J. Xiong, X. Lan, F. Li, W. Liu, and Q. Xi, "A 3D tracking algorithm of hypersonic gliding target based on kinematic modeling," *Syst. Eng. Electron.*, vol. 44, no. 1, pp. 63–71, 2022.
[25] J. Zhu, R. He, G. Tang, and W. Bao, "Pendulum maneuvering strategy for hypersonic glide vehicles," *Aerosp. Sci. Technol.*, vol. 78, pp. 62–70, Jul. 2018.
[26] A. Joshi, K. Sivan, and S. S. Amma, "Predictor-corrector reentry guidance algorithm with path constraints for atmospheric entry vehicles," *J. Guid., Control, Dyn.*, vol. 30, no. 5, pp. 1307–1318, 2007.
[27] K. Chen, L. Liu, and Y. Meng, *Launch Vehicle Flight Dynamics and Guidance*. Beijing, China: National Defense Industry Press, 2014, pp. 146–156.
[28] M. Sajjad, S. Khan, T. Hussain, K. Muhammad, A. K. Sangaiah, A. Castiglione, C. Esposito, and S. W. Baik, "CNN-based anti-spoofing two-tier multi-factor authentication system," *Pattern Recognit. Lett.*, vol. 126, pp. 123–131, Sep. 2019.
[29] X. Qing and Y. Niu, "Hourly day-ahead solar irradiance prediction using weather forecasts by LSTM," *Energy*, vol. 148, pp. 461–468, Apr. 2018.
[30] X. Shi, Z. Chen, H. Wang, and D. Yeung, "Convolutional LSTM network: A machine learning approach for precipitation nowcasting," in *Proc. 28th Int. Conf. Neural Inf. Proc. Syst.*, Nov. 2015, pp. 1–9.
[31] C. Wang, L. Ma, R. Li, T. S. Durrani, and H. Zhang, "Exploring trajectory prediction through machine learning methods," *IEEE Access*, vol. 7, pp. 101441–101452, 2019.
[32] L. Ma and S. Qu, "A sequence to sequence learning based car-following model for multi-step predictions considering reaction delay," *Transp. Res. C, Emerg. Technol.*, vol. 120, pp. 1–19, Nov. 2020.
[33] Z. Xiang, J. Yan, and I. Demir, "A rainfall-runoff model with LSTM-based sequence-to-sequence learning," *Water Resour. Res.*, vol. 56, no. 1, pp. 1–28, Jan. 2020.
[34] Z. Chen, M. Wu, R. Zhao, F. Guretno, R. Yan, and X. Li, "Machine remaining useful life prediction via an attention based deep learning approach," *IEEE Trans. Ind. Electron.*, vol. 68, no. 3, pp. 2521–2531, Mar. 2021.
[35] X. Chen, X. Xie, and D. Teng, "Short-term traffic flow prediction based on ConvLSTM model," in *Proc. IEEE 5th Inf. Technol. Mechatronics Eng. Conf. (ITOEC)*, Jun. 2020, pp. 846–850.
[36] B. Li, B. Tang, L. Deng, and M. Zhao, "Self-attention ConvLSTM and its application in RUL prediction of rolling bearings," *IEEE Trans. Instrum. Meas.*, vol. 70, pp. 1–11, 2021.
[37] W. Zeng, Z. Quan, Z. Zhao, C. Xie, and X. Lu, "A deep learning approach for aircraft trajectory prediction in terminal airspace," *IEEE Access*, vol. 8, pp. 151250–151266, 2020.

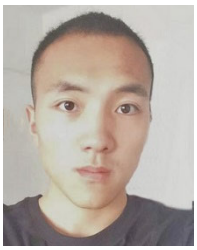

JUNBIAO ZHANG received the B.S. degree from the Xi'an University of Science and Technology, in 2016, and the M.S. degree from the Army Academy of Artillery and Air Defense, in 2018. He is currently pursuing the Ph.D. degree with the Air Force Early Warning Academy. His research interests include target detection and tracking and trajectory prediction.

JIAJUN XIONG received the Ph.D. degree in software engineering from the Huazhong University of Science and Technology, in 2004. Currently, he is a Professor with the Air Force Early Warning Academy. His research interests include data fusion and early warning intelligence analysis.

LINGZHI LI received the M.S. degree from the Air Force Early Warning Academy, in 2005. Currently, she is an Associate Professor with the Department No.4, Air Force Early Warning Academy. Her research interests include multi-sensor data fusion and information systems.

QIUSHI XI received the B.S. and M.S. degrees from the Air Force Radar Academy, Wuhan, Hubei, in 2003 and 2006, respectively. Currently, she is a Lecturer with the Air Force Early Warning Academy. Her research interests include computer science and technology, hypersonic missile defense strategy, and information fusion.

XIN CHEN received the Ph.D. degree in cryptology from the National University of Defense Technology. He is currently an Associate Professor with the Air Force Early Warning Academy, Wuhan, China. His research interests include big data analysis and cloud computing.

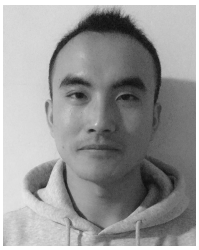

FAN LI received the B.S. and M.S. degrees in radar engineering and signal processing from the Air Force Early Warning Academy, Wuhan, China, in 2014 and 2017, respectively. Currently, he is an Engineer with 95980 Unit. His research interests include target detection and tracking and nonlinear filtering.